This is a post-print version of
Tsubaki, R., Baranya, S., Muste, M. and Toda, Y. (2018), Spatio-temporal patterns of sediment particle movement on 2D and 3D bedforms. Experiments in Fluids. 59(93), Accepted Author Manuscript. DOI: 10.1007/s00348-018-2551-y

The final publication is available at
https://doi.org/10.1007/s00348-018-2551-y

Spatio-temporal patterns of sediment particle movement on 2D and 3D bedforms

Ryota Tsubaki[a*], Sándor Baranya[b], Marian Muste[c] and Yuji TODA[d]

[a] Associate Professor, Department of Civil and Environmental Engineering, Nagoya University, Furo-cho, Chikusa-ku, Nagoya, 464-8603 Japan
(Tel: 81-52-789-4625, e-mail: rtsubaki@civil.nagoya-u.ac.jp)
[b] Associate Professor, Department of Hydraulic and Water Resources Engineering, Budapest University of Technology and Economics, (Tel: 36-1-463-1686, e-mail: baranya.sandor@epito.bme.hu)
[c] Research Engineer, IIHR-Hydroscience & Engineering, University of Iowa
(Tel: 1-319-384-0624, e-mail: marian-muste@uiowa.edu)
[d] Professor, Department of Civil and Environmental Engineering, Nagoya University, Furo-cho, Chikusa-ku, Nagoya, 464-8603 Japan (Tel: 81-52-789-5176, e-mail: ytoda@cc.nagoya-u.ac.jp)
* Corresponding author.

Abstract

An experimental study was conducted to explore sediment particle motion in an open channel and its relationship to bedform characteristics. High-definition submersed video cameras were utilized to record images of particle motion over a dune's length scale. Image processing was conducted to account for illumination heterogeneity due to bedform geometric irregularity and light reflection at the water's surface. Identification of moving particles using a customized algorithm was subsequently conducted and then the instantaneous velocity distribution of sediment particles was evaluated using Particle Image Velocimetry. Obtained experimental results indicate that the motion of sediment particles atop dunes differs depending on dune

geometry (i.e., two-dimensional or three-dimensional, respectively). Sediment motion and its relationship to dune shape and dynamics are also discussed.

Keywords: sediment particle motion; dune; dune migration; PIV

1 Introduction

Dunes naturally develop in sand-bed rivers leading to substantial changes in flow resistance and sediment flux. Dunes are an integral part of river bed morphology and, in contrast to ripples, are typically described as moving in the streamwise direction with little change in transverse flow direction. Ripples are regarded as relatively small-scale undulations occurring atop dunes with a more irregular geometry as compared to dunes. Most available investigations consider dunes as two-dimensional bed features irrespective of their actual geometry. Example investigations include theoretical analyses (e.g. Nelson and Smith, 1989), laboratory experiments (e.g. Bennett and Best, 1995; Kadota and Nezu, 1999; Chichibu et al., 2008) and numerical simulations (e.g. Giri and Shimizu, 2006; Yue et al., 2006; Paarlberg et al., 2006; Niemann et al., 2011).

In contrast to previous studies, here, we distinguish between dunes with a considerable change in geometry in the transverse flow direction and label them as three dimensional, and dunes with smaller changes in this direction and label them as two dimensional. Our approach is similar to the dune characterization approach used by Venditti et al. (2005) and Venditti (2007). This distinction has been facilitated by more accurate dune tracking technologies that have become available for laboratory and field conditions. For example, the use of multi-beam sonar or aerial Light Detection and Ranging (LiDAR) enabled us to not only determine dune geometrical characteristics but dune migration speed. The latter aspect can be estimated by analyzing maps created by such point-wise or point-cloud sounding methods (e.g. Simons et al., 1965; Engel and Lau, 1981; Kostaschuk et al., 1989; Dinehart, 2002; Gray et al., 2010, Muste et al., 2016). The determined dynamic characteristics of dune migration can be related to bed-load flux (Mohrig and Smith, 1996). The availability of these new measurement approaches has led to new perspectives for understanding the dynamics of dune dynamics and their interactions with flow over alluvial dunes, as well as other practical measurements as demonstrated by Abraham et al. (2011), Heath et al. (2015), Muste et al. (2016) and Koseki et al. (2017).

The opportunities such new technologies offer in shedding light on the fluid dynamics of river dunes was critically reviewed by Best (2005) who identified five key areas of recent/ongoing and future research. One of these areas is the influence of dune spatial configuration on overall bedload transport. Initial results were provided by Maddux et al. (2003a) who demonstrated that three-dimensional dunes display 50% larger friction coefficients than conventionally assumed, while turbulent intensity decreases as compared to two-dimensional dunes due to the generation of secondary flows over three-dimensional forms. Additionally, Zedler and Street (2001) used a large-eddy simulation model coupled with a sediment transport model to observe flow features over two-dimensional and three-dimensional ripples. The closest study to our investigative approach is the study of Palmer et al. (2012) who used laser-light sheet Particle Image Velocimetry (PIV) to observe the flow field above the stoss- and lee-sides of barchan dunes in a vertical plane aligned with the main flow direction.

While progress has been made in the approach for observing various flow scales (from particle to dune scales), previous experimental studies were performed on fixed beds. Therefore, the possibility of extending inferences to actual rates of sediment transport was not possible. The objective of our study was to correlate sediment transport, sediment flux, and bed topography migration over two-dimensional and three-dimensional bedforms formed in an open-channel with a sand bed based on a consideration of fine (i.e., at the level of individual particles) to larger (i.e. over a dune's length) scale variations. Below, we discuss the relationship between the time-averaged and, especially, time variation of the sediment transport velocity distribution and the migration of dune shapes.

2 Experimental setup

In this section, we describe the experimental set-up including flume properties, sediment material, the investigated flow conditions, and the video capturing system. Image pre-processing, PIV, and post-processing methods are subsequently presented.

2.1 Flume and sediment

The dimensions of the experimental flume used in the study was 5 × 0.762 × 0.3 m^3**,** corresponding to the flume length, width, and sidewall height, respectively. The channel slope was set at 0.3%. The channel bed consisted of well-sorted coarse sand (d_{50} = 0.6 mm) covering the flume bed over 5 cm (2 inches). To trigger fully turbulent flow, a porous medium (coarse plastic sponge) and grids were installed over 1.0 m of the flume entrance. Since the experimental facility had no sediment recirculating system, the following 1.5 m section of the flume was used to feed the flow with sediment. During the course of experiments, slight degradation of the sediment supply section of the flume was observed. To ensure that sediment movement in the test area was close to natural conditions, sand was continuously supplied from the sediment supply section during experiments. Six-hour-long experiments were conducted for each experiment beginning from a flat-bed until the test section developed a flow and bed in equilibrium. Equilibrium was tested by checking flow uniformity within the measurement section (using piezometers distributed along the flume) and visual observations.

2.2 Flow conditions

Two flow cases characterized by the flow parameters, as summarized in Table 1, were established. The flow cases are identical to those used in Muste et al. (2016), whereby measurements with an ultrasonic-depth-sounder array (Multiple Transducer Array: MTA) were conducted. Namely, the 3D-bed and 2D-bed cases correspond to Run 2 and Run 3 in Muste et al. (2016), respectively. Fig. 1 displays channel bathymetry as quantified using a MTA. In the 3D- and 2D-bed cases, the flow rate, Q, differs by approximately 10%, while the difference in sediment rates, q_B**,** was more than double. Mean dune heights were approximately 0.01 to 0.015 m, with differences in their spatial distribution. The 3D-bed case displays complex, three-dimensional topography, whereas bedform migration in the 2D-bed case is characterized by a more uniform pattern in the spanwise direction. In the preliminary experiment, Run 2 was repeated three times and, as shown in Fig 1a, a quite random bedform was determined. Run 3 was repeated four times and a similar bedform, dune length/height, and sediment rate were observed. The migrating speed of the bedform was approximately double for the 3D-bed case (Run 2) as compared to the 2D-bed case (Run 3) (see Muste et al., 2016). In Fig. 1, regions analyzed in this study are indicated using rectangles.

Table 1 Flow parameters.

	Q (m^3/s)	B (m)	H (m)	U (=Q/BH, m/s)	Fr ($U/\sqrt{gH}$)	I_{bed}	τ (=ρgHI_{bed}, N)	u_* (=$\sqrt{\tau/\rho}$, m/s)	Re_* (=u_*d/ν)	$\tau_{*\text{bulk}}$ (=$\tau/\rho sgd$)	q_B (kg/m/h)
3D-bed case (Run 2)	0.0198	0.762	0.095	0.27	0.28	0.003	2.80	0.0529	31.8	0.29	0.99
2D-bed case (Run 3)	0.0181	0.762	0.09	0.26	0.28	0.003	2.65	0.0515	30.9	0.27	0.44

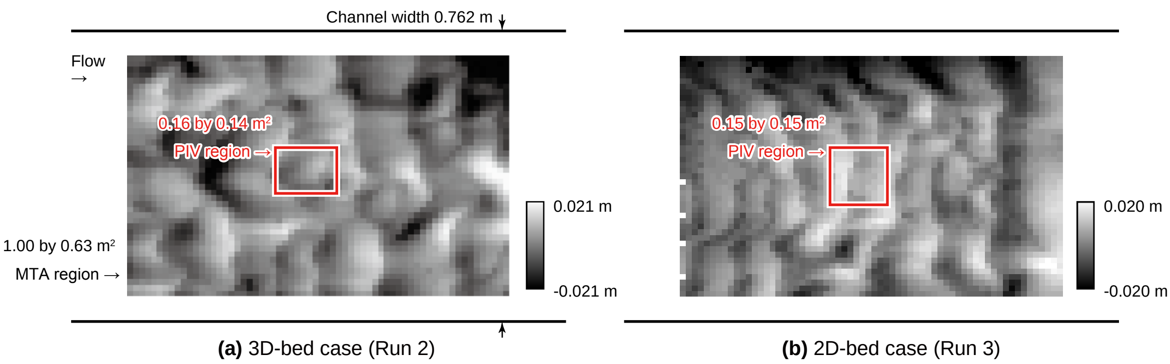

Fig. **1**. Snapshots of the MTA bed elevation distribution illustrated using a gray scale (Muste et al., 2016). MTA and PIV measurements were conducted at equilibrium flow but not simultaneously.

2.3 Video camera and lighting

To avoid interference from water surface waviness, two action cameras (Model AS30V, Sony Co.) with waterproof covers were fixed on the water's surface to keep the camera lens submerged (Fig. 2). To ensure strong illumination for the area under analysis, we developed submersed light-emitting diode (LED) modules. Each LED light consisted of a high power 800 lumens 10 W LED chip and a 5 × 5 cm^2 aluminum heat spreader. Each LED light source was protected by a transparent resin cover to make it waterproof. The light modules we developed were flat (1 cm thick), were placed on the flat side parallel to the flow direction, and were located downstream and close to the walls. The above-mentioned configuration for the image recording and illumination components were designed to encompass a stoss-crest-lee-trough spatial sequence (i.e., a dune wavelength) in one image while reducing water flow and sediment motion disturbance in the recording area as much as possible (Detert et al., 2010; Cecchetto et al., 2016).

Images were recorded at 120 frames per second (FPS) in 1280 by 720 pixels and encoded in MPEG-4 AVC/H.264 format. After obtaining the images for 75 seconds, cameras and lights were rapidly removed from the water. The dimensions of the submersed lens cover for one camera were approximately 6.5 × 7 cm^2 and the camera captured sediment particle motion developing over an area of 20 × 10 cm^2. To cover a consecutive 20 × 20 cm^2 region of the channel bed, as shown in Fig. 3, the two cameras were aligned in the spanwise direction. Pixel resolution was fine enough to identify sediment particles. However, due to too short a focal length, the presence of air bubbles, and the turbidity and limited transparency of the lens cover, not all of the particles were identifiable. To obtain the horizontal, two-component velocity distribution of an area wide enough to cover the dune wavelength, the images acquired for each strongly illuminated area were subsequently analyzed using a Particle Image Velocimetry (PIV) approach. The positions of crests and troughs are depicted in Fig. 3 using white and black lines, respectively. The figure substantiates the difference in bed geometry between the two cases. In the 3D-bed case, the dune fronts are randomly located and not continued while in the 2D-bed case the dune crests and troughs are continuous and orthogonal to the flow direction.

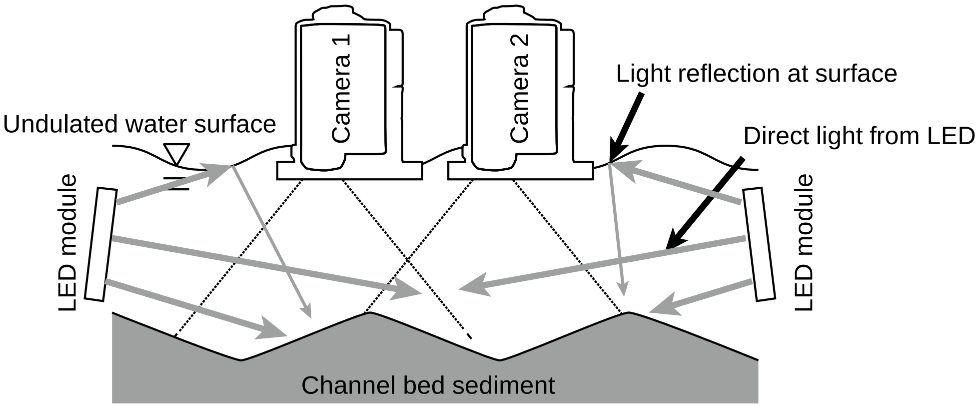

Fig. **2**. Schematic of the image recording experimental arrangement (streamwise cross section).

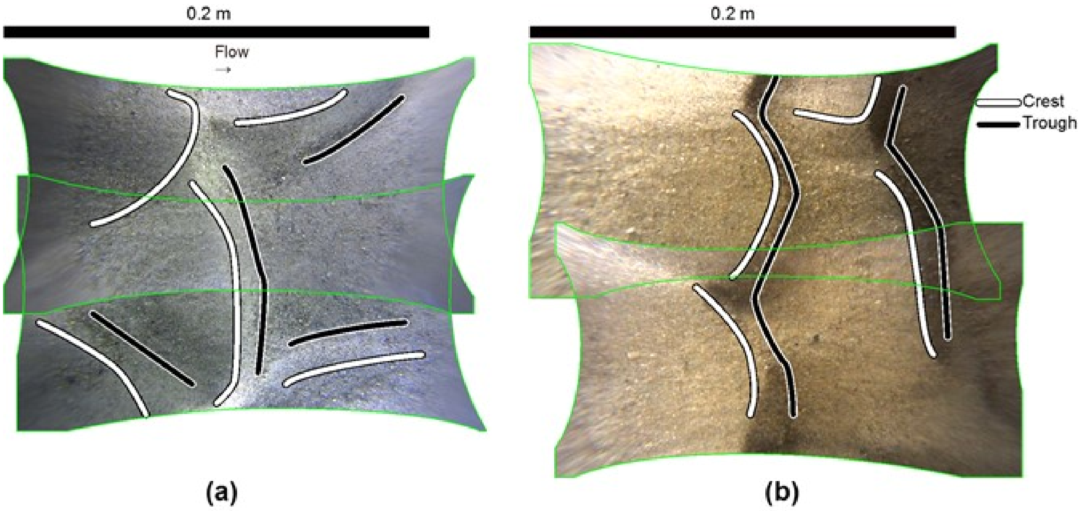

Fig. **3**. Bedform reconstructed from two overlapping video recordings: **a)** 3D-bed case, **b)** 2D-bed case.

3 Image processing

3.1 Image Conditioning and Pre-processing

Time stamps of the recording from the two cameras were manually synchronized by comparing the movement of sand particles in the overlapping area of two cameras (see Fig. 3). Then, as described below and as illustrated in Fig. 4, a three-step protocol for both enhancing the image of moving particles was developed. The protocol was applied to all of the images prior to processing images using the PIV software.

Step 1: Level equalization. To remove the spatial bias in luminance level due to bed undulation and lighting irregularity, the image luminance level was equalized using specific window sizes. The local average and the standard deviation of luminance within the window were calculated and luminance at the center of the window was normalized using the average and standard deviation. Figs. 4**c**, **d**, and **e** display the tested window sizes (i.e., 8 × 8 pixels, 16 × 16 pixels and 32 × 32 pixels). Comparisons indicated that the 16 × 16 pixels (corresponding to approximately $3.5d_{50} \times 3.5d_{50}$) were the best in removing spatial bias due to luminance level differences.

Step 2: Time-series change analysis. A pointwise luminance change for consecutive frames was observed, and the maximum and minimum for the extracted time-series luminance were obtained. The instantaneous pointwise luminance was then calculated from the deviation of the instantaneous pointwise luminance based on the maximum/minimum from consecutive frames (see Figs. 4**h** and **j** as examples). As compared in Figs. 4**g**, **h**, and **i** for 2, 4, and 16 frames, respectively, we tested the sensitivity of the number of frames. Based on comparisons, we decided that four frames were the optimum number for highlighting the shape of moving sediment particles.

Step 3: Image rectification. Image coordinates for two camera angles were rectified by assuming that the channel bed was flat (see Figs. 4**m** to **p**) and images from the two cameras were combined to obtain a composite image spanning an area of approximately 20 × 20 cm^2 (Fig. 4**q**). The distance between the lens cover to the channel bed was 0.09 m. Therefore, one pixel corresponds to 0.13 mm. Given that the sediment grain size for the bed material was d_{50} = 0.6 mm, one sediment particle diameter corresponds to roughly four pixels in the original image. The channel bed height varied by approximately 0.01 m and this bed undulation was not accounted for during rectification. The saltation height of moving grains was less than 0.005 m. Such vertical displacement could not be accounted for in the image rectification. Given that the cameras used to obtain images produced a considerable distortion on the image periphery, only the central region spanning an area of 15 × 15 cm^2 was used for PIV processing. The peripheral of the PIV region possibly contains up to a 0.5 cm location bias error that is proportional to bed undulation. Images acquired from the two camera locations were overlapped such that the transverse component of the bias error in the overlapping region was canceled out of the data. Movement of the bedform was recorded for 75 seconds (corresponding to 9,000 frames) and was subsequently analyzed for inferring particle dynamics. Since our focus was on particle migration patterns relative to the bedform (i.e., sediment grain motion on the dune), displacement of the bedform during the 75 seconds of recording were taken into account in our data. To fix the locations of crests and troughs in the mosaic images used for the PIV analysis, we offset this migration. As described in Muste et al. (2016), the average speed for a migrating dune was estimated using MTA measurements.

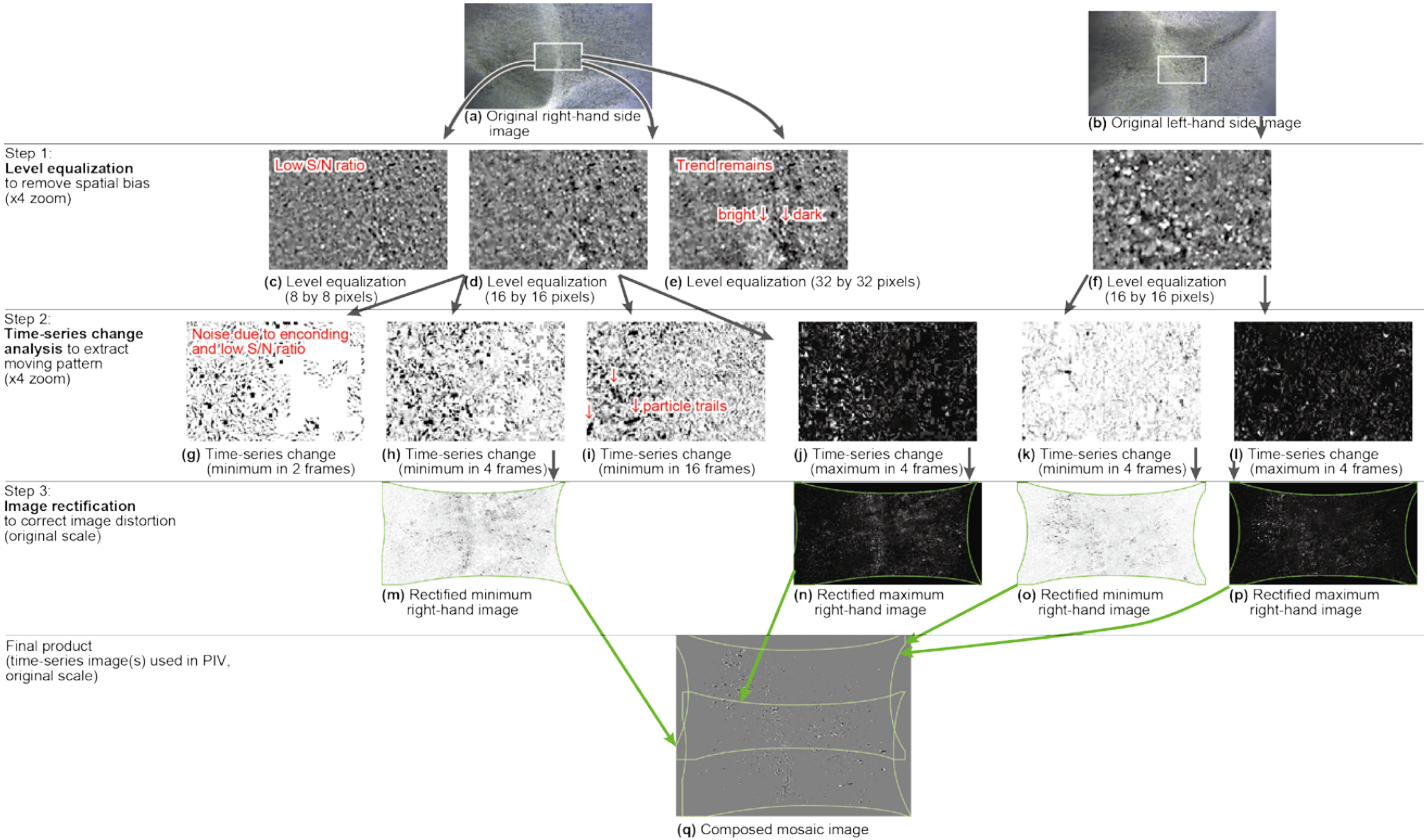

Fig. **4**. Protocols for conditioning and pre-processing images for the PIV analysis. Note that the brightness level in subfigures (c) to (q) was modified to improve visual appearance to the eye and that the central region was clipped in subfigure (c) to (l) to improve visualization of the details.

3.2 Particle Image Velocimetry processing

Adjacent sections of the channel bed spanning areas of 16 × 12 cm^2 and 15 × 15 cm^2 were analyzed using the PIV for the 3D- and 2D-bed cases, respectively, using an in-house Large-Scale PIV (LSPIV) software package (Tsubaki and Fujita 2005, Tsubaki et al. 2008; Tsubaki et al. 2011; Gunawan et al. 2012). The interrogation area used to calculate the instantaneous sediment velocity distribution was 50 × 50 pixels (0.75 × 0.75 cm^2). Using the conventional approach of processing with PIV, due to limited image quality, two consecutive frames recorded at 120 frames per second provided noisy instantaneous velocity distributions. Factors limiting image quality include imperfect focus due to short focal distance, complex optical conditions, and noise due to MPEG4 encoding. Coping with this limitation was determined by adopting the ensemble correlation PIV approach (Westerweel et al. 2004). In this method, the ensemble-average of cross-correlation distributions obtained for ten consecutive frame pairs was calculated and the peak of the ensemble-averaged cross-correlation was used to estimate local and instantaneous velocity at the corresponding interrogation area. Ensemble correlation PIV is a method suitable for an image set recorded with high spatial and temporal resolutions relative to the scale of turbulence. Since our focus was to discuss sediment particle motion driven by coherent turbulence near a river bed and since images were recorded using substantially higher spatial and time resolutions as compared to scales of coherent turbulence driving sediment motion, measurement conditions in the present study are a better fit to the ensemble correlation PIV. Since we used the PIV approach and since the amount of moving grains could not be directly counted, bedload fluxes were not determined based on the PIV results.

The moving grain pattern was extracted using the image pre-processing steps described in Section 3.1 and image areas without sediment motion contained no image patterns. Computationally, this type of region tends to display a low peak cross-correlation, a low spatial deviation of luminance, and either a zero or an erroneous velocity value is obtained by applying PIV to such regions. After processing the images using PIV, the statistics for the time-series velocities at each interrogation area were obtained using two approaches. In the first approach, velocities in no-particle-motion areas were neglected when calculating statistics. In the second approach, zero was assumed for velocities within the no-particle-motion areas. Based on the objective of each statistics calculation, the two approaches were further used in the analysis.

4 Results

4.1 Vector field consistency check

To check the suitability of the recorded images and PIV performance in tracking grain particle dynamics over the duration of recordings, sample image frames from the beginning (just after the submergence of the image capturing system) and at the end of the video recording were analyzed. For the 3D-bed case, the PIV result for images recorded over 17 seconds (2,000 frames) at the beginning were compared with results from images recorded over the last 42 seconds (5,000 frames). The PIV results are compared in Fig. 5. In this figure, the mean and standard deviation for the velocities were calculated at all locations, except in areas/instants of no-particle-motion. As observed in the figure, in this experiment, the spatial distribution of the average and standard deviation for the velocity field was relatively similar at the beginning and end of image recording. The similarity led to the following inferences: (1) the proximity of the cameras and the lighting system did not affect sediment movement, (2) the PIV measurements were consistent; and (3) the 75-second recording length was long enough to capture the statistics of bed movement dynamics. The first inference was observed to avoid the experimental issues pointed out by Detert et al. (2010) and Cecchetto et al. (2016).

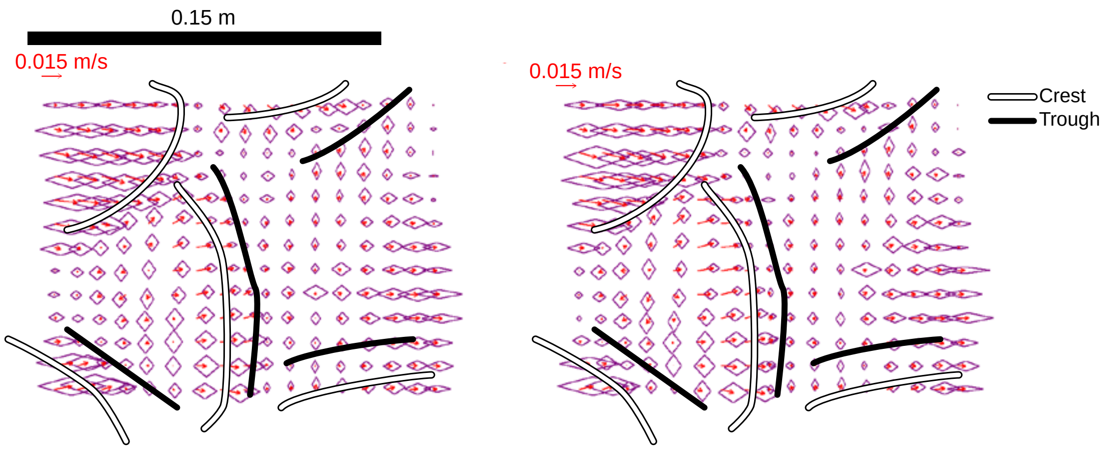

(a) Result from first 2000 frames of 3D-bed case **(b)** Result from last 5000 frames of 3D-bed case

Fig. **5**. A comparison of the averaged and standard deviations of the velocities calculated at the beginning **(a)** and end **(b)** of the 3D-bed case recording. Vectors in the plots indicate the mean velocity. The horizontal and vertical axes lengths of the diamonds indicate the two-fold standard deviation of velocity components for each calculated vector.

4.2 Time-averaged sediment velocity distributions

Fig. 6 provides a comparison between the time-averaged velocity distributions of moving sediment particles calculated from the entire recording (total of 9,000 frames) for the 3D- and 2D-bed cases. The result for 3D-bed case shows complex streamwise and lateral sediment movement commensurate with the geometry on dunes on which the particles are moving. On the stoss-side of crests, the sediment particles migrate orthogonal to the crest-line, as indicated by area (1) in Fig. 6**a**. Movements opposite to the flow direction were observed for particles located at the tow of the crest on its lee side region (2) in Fig. 6. Distinct spanwise movement can be found in regions labeled with (3) in the same figure. As illustrated in Fig. 6**b**, the velocity of sediment particles along dunes for the 2D-bed case was quite uniformly aligned with the streamwise direction. Region (4) in Fig. 6**b** where velocities converged to a common location is evident. As seen in Fig. 3**b**, Region (4) corresponds to a dent in the two-dimensional crest where a depression of the bed is visible.

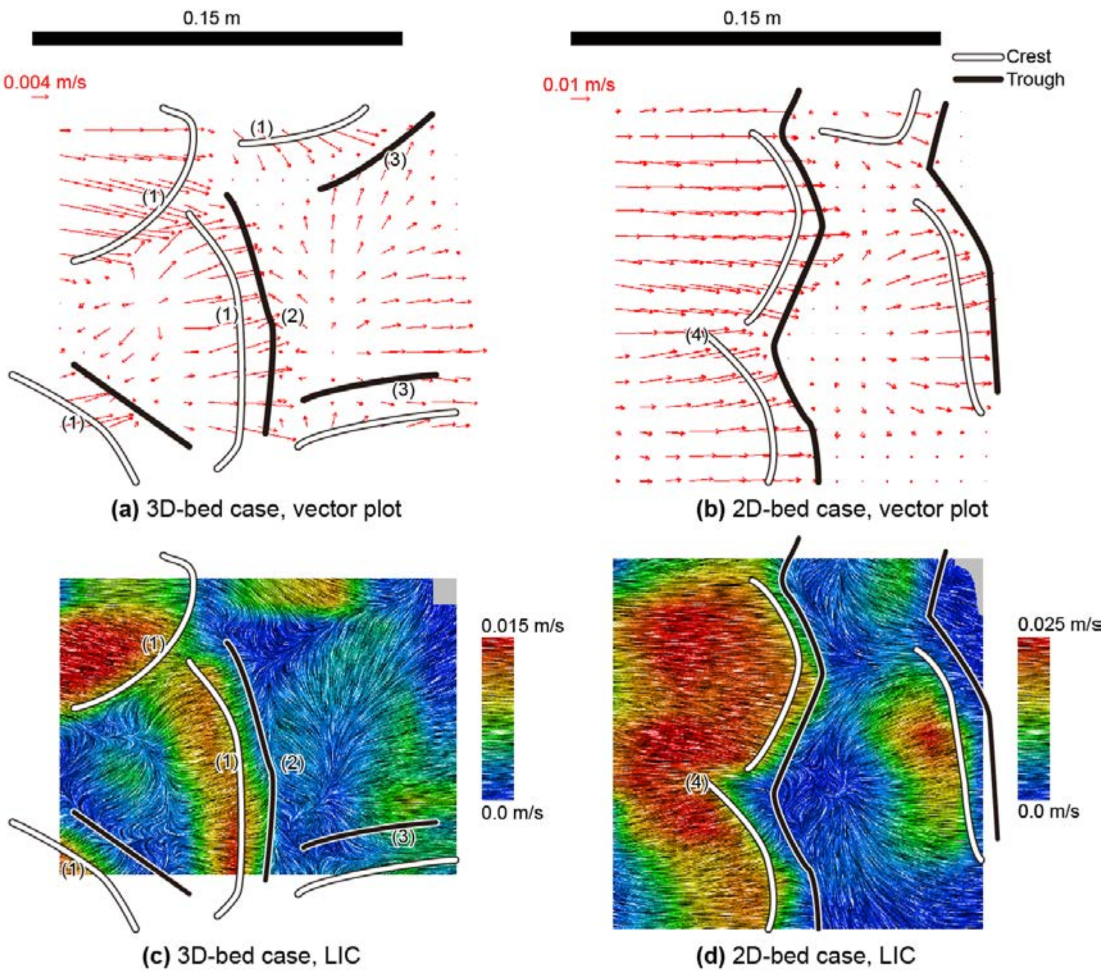

Fig. **6**. The time-averaged velocity distribution of moving sand particles (no-particle-motion areas/instants are assumed to have 0 m/s when calculating statistics): **a)** a vector plot for the 3D-bed case; **b)** a vector plot for the 2D-bed case; **c)** a line integral convolution (LIC, Cabral and Leedom 1993) for the 3D-bed case; and **d)** a LIC for the 2D-bed case. The direction of the texture in LIC plots corresponds to the local velocity direction. The contrast (color for colored figure) of the texture correlates with the local velocity magnitude.

4.3 Sediment velocity time-series at fixed points

Another aspect of the dynamics of moving sediment grains can be observed by visualizing the time series of velocities passing through specific locations. For this purpose, four locations on the bedform (i.e., points T1, C1, T2, and C2 in Fig. 7) were selected over a dune length. A comparison of the velocity magnitude and its variability over time illustrates that particles exhibit a distinct behavior in response to the type of turbulent flow occurring at specific points over the dune. The comparison is especially important for the trough portion of the bedform (see the dashed-black and solid-black lines) where both positive and negative velocity components were intermittently recorded and where no obvious specific interval of a velocity change was observed. A more specialized analysis is presented in the next section for extracting spatio-temporal features from such complicated velocity fields.

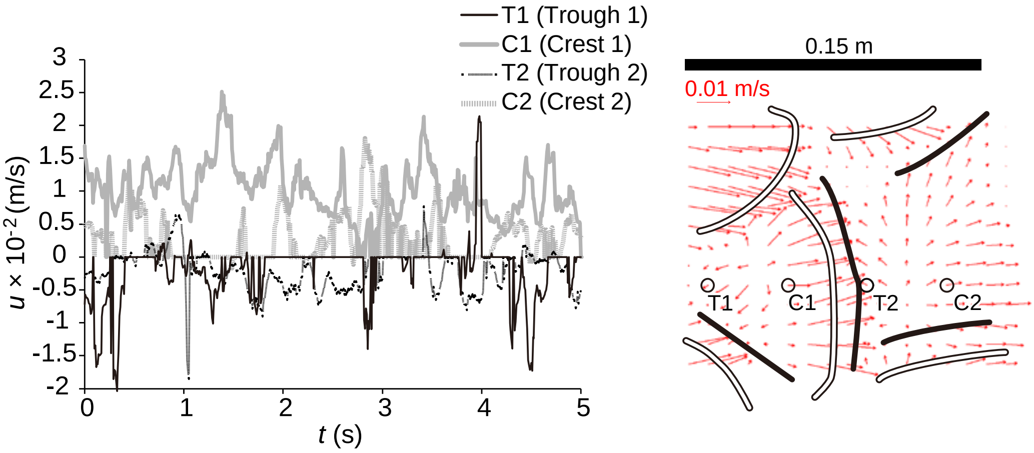

Fig. **7**. A time-series of the streamwise velocity component of sand particles acquired at fixed points (no-particle-motion areas/instants are assumed to have 0 m/s).

4.4 Proper Orthogonal Decomposition (POD) of the sediment velocity field

Several methods are used for defining, detecting, and quantifying coherent structures in turbulent flows. The Proper Orthogonal Decomposition (known as the POD) is a widely used method for extracting structures from a complicated spatio-temporal data set. Examples of the POD application include open-channel flows, jets, and wakes created behind bluff bodies (Constantinescu et al., 2017). POD defines the most energetic modes of motion (see, for example, Hilberg et al., 1994; Feng et al., 2011; Wang et al., 2015; Sokoray-Varga, 2016). Following the notations used in Wang et al. (2015), the spatio-temporal fluctuating velocity distribution $\boldsymbol{u}(\boldsymbol{x}, t)$ is reconstructed by products of the spatial pattern, $\Phi_n(\boldsymbol{x})$, and the amplitude coefficient, $a_n(t)$, for Mode n as:

$$\boldsymbol{u}(\boldsymbol{x},t)=\sum_{n=1}^{N}\boldsymbol{\Phi}_n(\boldsymbol{x})a_n(t), \quad (1)$$

where $\boldsymbol{x}$ is the coordinate vector, t is the time, and N is the total mode number. The contribution ratio, c, for Mode n is defined as:

$$c_n=\frac{\lambda_n}{\sum_{k=1}^{N}\lambda_k} \quad (2)$$

and λ_n is the n-th largest eigenvalue of the correlation matrix:

$$R_{xy}=\sum_t \boldsymbol{u}_{xt}\boldsymbol{u}_{yt}^{T}. \quad (3)$$

The POD technique was added to the processing stage of the experimental protocol in this study to illustrate the full sequence of protocols from data acquisition to the final analysis and are relevant for this type of study.

Inferences from the POD analysis, as applied to the obtained data, are discussed below. Fig. 8 displays a spatial plot of the upper three modes extracted from each case. The upper half plots provide results from the 3D-bed case while the lower half plots the 2D-bed case. The crest contour was overlain for easier spatial referencing of vectors with various areas of activity. The three selected modes for the 3D-bed case display flow accelerations on the upper-left and lower-left dune crests. In Mode 1 (Fig. 8**a**), velocity on the two crests (indicated with label (i) in the figure) are opposite in direction, indicating that sediment acceleration occurred on both crests but not simultaneously. In Mode 2 (Fig. 8**b**), the movement of sediment particles on the same crests (labeled (ii) in the figure) is synchronous. The synchronized sediment movement is relatively small (with a contribution ratio of 16%) as compared to Mode 1 (with a contribution ratio of 19%), corresponding to sediment acceleration occurring on one crest. Mode 3, as illustrated in Fig. 8**c**, displays sediment movement in the trough area (labeled (iii) in the figure). The time-averaged velocity distribution shown in Fig. 6**a** indicates a diverging pattern for sediment migration, including moments with reverse flow on the stoss side of dunes (at the center of the three (1)s in Fig. 6**a**). No indication of reverse flow or diverging patterns in found the Figs. 8a, b, and c for the upper POD modes. Therefore, the conclusion is that sediment transport on the dune crest is more dynamic with respect to time as compared to sediment flow changes on the stoss faces.

The result for the 2D-bed case, as shown in the lower half of Fig. 8, suggests that Mode 1 is quite active with a relatively large contribution ratio (i.e., 39%) over the entire crest area (indicated with the label (iv)s in Fig. 8**d**). The finding indicates that during the 2D-bed case sediment transport on the crest was simultaneous and strong, in contrast with the 3D-bed case.

Particle movement in Modes 2 and 3, as illustrated in Figs. 8**e** and **f**, is quite different from Mode 1, and Modes 2 and 3 are associated with sediment movement on the individual crests. For the 2D-bed case, the contribution ratios for Modes 2 and 3 are substantially lower than that of Mode 1, indicating that the activation of sediment transport on the individual crest is relatively minor, in contrast to the result for the 2D-bed case.

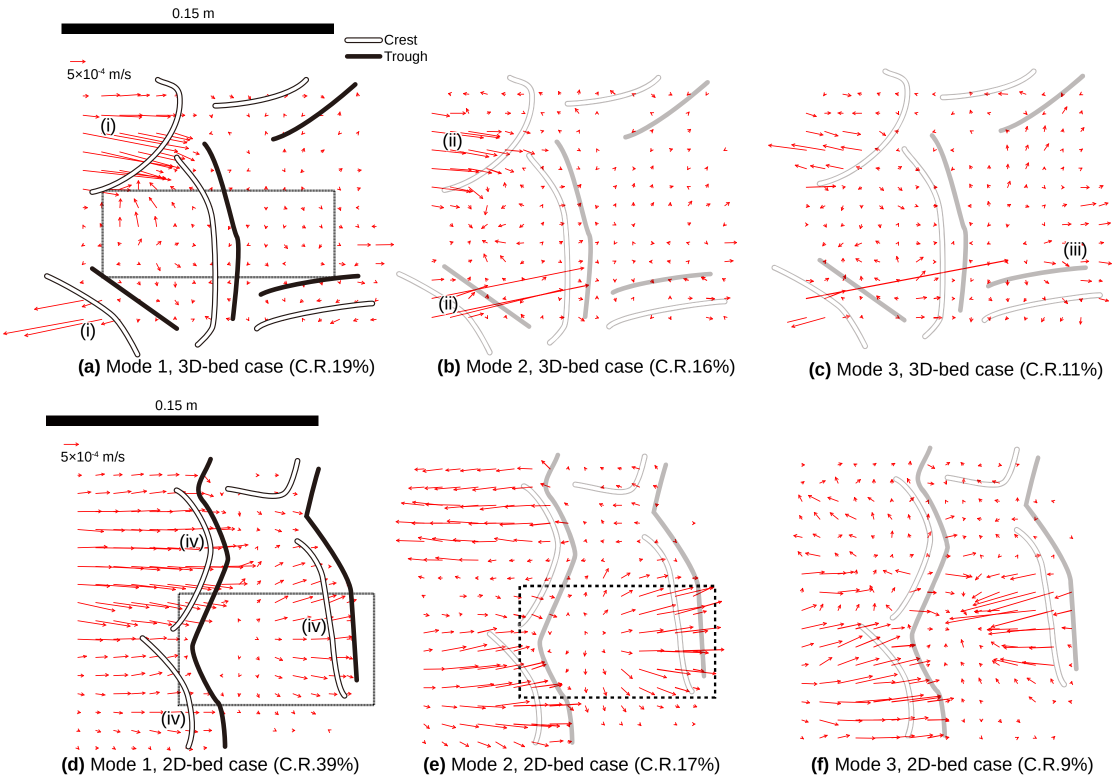

Fig. **8**. Spatial patterns, *Φ*, of the top three modes extracted with the POD analysis applied to grain velocities. The contribution ratio (C.R.) for each mode is indicated in the figure's caption. The dashed-line rectangle in Fig 8**a** displays the boundary of the discussion illustrated in Fig. 11. A typical diverging pattern is observed in the dashed-line rectangles in Figs 8**d** and **e**.

Fig. 9 displays the time variation of the amplitude coefficients corresponding to the upper three modes for the 3D- and 2D-bed cases. The lack of discernable patterns in plots of the mode fluctuations and the lack of a representative period is similar to the time series of the raw velocity components shown in Fig. 7. Despite the lack of a distinct repeated pattern, the plots in Figs. 7 and 9 illustrate flow "bursts" acting on the sediment that are less than one second. Furthermore, flow bursts in the 3D-bed case are shorter than those in the 2D-bed case. Sediment flux in the 3D-bed case was more than double as compared to those in the 2D-bed case, so the active bursts observed in the 2D-bed case did not result in active sediment transport.

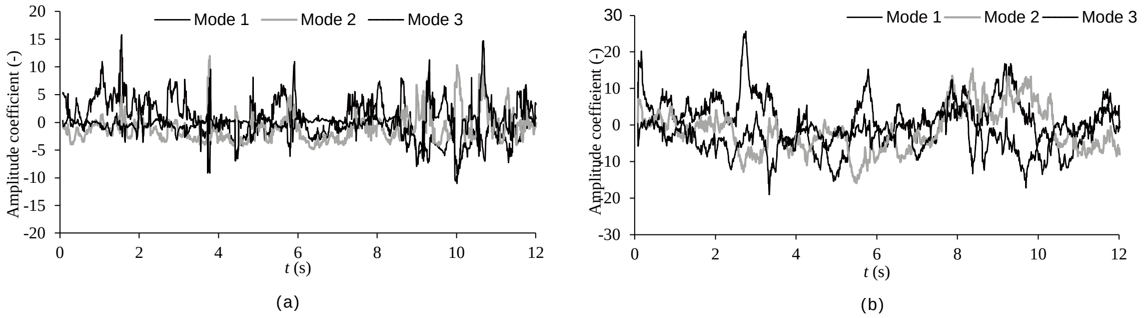

Fig. **9**. A time-series of the amplitude coefficients, *a*, for the three motion Modes: **a)** 3D-bed case, **b)** 2D-bed case.

Fig. 10 provides phase-space projections of the amplitude coefficients between the three modes of the 3D-bed case. If these projections visualize some specific patterns they are indicative of some sort of movement organization. For example, for a situation where the propagating wave is composed of two modes, the phase-space projection displays a circular pattern (e.g. the left plot of Fig. 6 in Cizmas et al. 2003). An inspection of phase-space projections for the 3D-bed case reveals persistence in the Mode-1-Mode-2 (Fig. 10**a**) and Mode-2-Mode-3 plots (Fig. 10**c**). Such patterns indicate a negative amplitude coefficient for Mode 2 when the amplitude coefficients for Modes 1 and 3 are almost zero and a positive amplitude coefficient in Mode 2 when a considerable large variation of the amplitude coefficient occurs for Modes 1 and 3. The result suggests the controlling role played by Mode 2 on the status of Modes 1 and 3, even if the contribution ratio of Mode 2 is smaller than that of Mode 1. The spatial pattern for Mode 2 shows acceleration on the dunes (ii) in Fig. 8b, whereas the negative amplitude coefficient for Mode 2 corresponds to deceleration over the same areas.

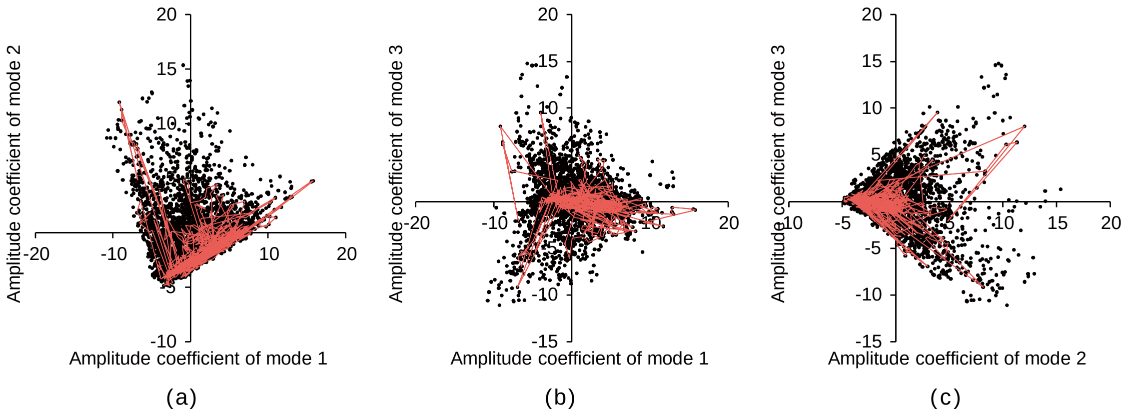

Fig. **10**. Phase-space projections for the amplitude coefficients, *a*, of the motion Modes analyzed for the 3D-bed case. The first 1,000 points for each diagram are connected by a line to substantiate the evolution of the phase-space location in time.

Fig. 11 shows POD modes for the 3D-bed case evaluated within the area of the velocity field containing a stoss-crest-lee-trough-stoss spatial sequence (see the dashed-line rectangle in Fig. 8**a**). Diverging patterns for sediment motion and reverse velocities on the stoss side of dunes in the first mode (see Fig. 11**a**) were determined in this region. Converging flow patterns were extracted for the motions in Mode 3 (Fig. 11**c**). Sediment diversion on the stoss of dunes was also observed in the time-averaged velocity fields illustrated in Figs. 6**a** and **b** and the POD modes illustrated in Figs. 8**d**, **e** (indicated with the dashed-line rectangles), and 11**a**. Diversion was not clearly substantiated in the visualization of major motion Modes in the velocity field for the 3D-bed case (Fig. 8**a** to **c**). As a result, the sediment transport pattern for each stoss-crest-lee-trough sequence may be universal for both two-dimensional and three-dimensional bedforms but randomness in time in sediment migration is a feature that only characterizes the three-dimensional bedform and is absent in the two-dimensional case.

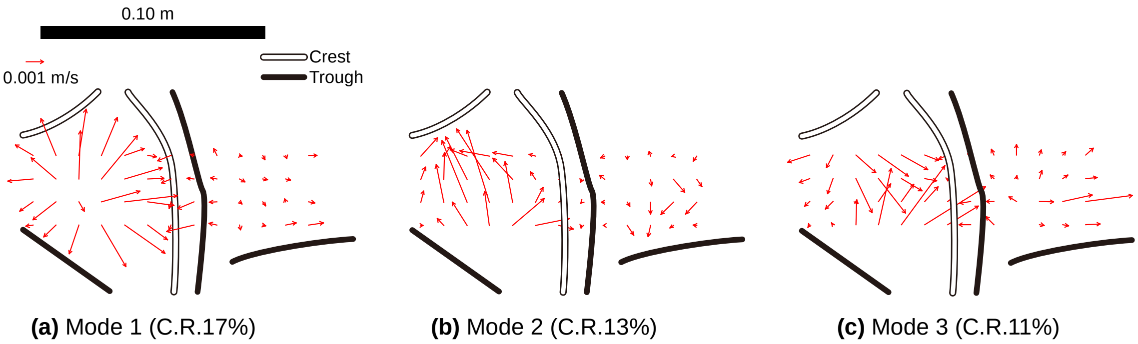

Fig. **11**. The spatial patterns, *Φ*, of the top three motion Modes extracted for the area indicated as the dashed-line box in Fig. 8a (a consecutive crest-trough sequence for the 3D-bed case).

4.5 Summary

In this study, we determined distinct behavior for particle dynamics over two- and three-dimensional bedforms with a continuous interaction between the flow and its moving boundary condition. The 3D-bed case was characterized by sporadic sediment transport events occurring on each individual crest. An obvious time discontinuity for crest-stoss movement in the 3D-bed case as compared to the 2D-bed case was revealed. The result is indicated by the divergence of sediment movement on stoss faces and their lack of active sediment movement on crests. On the other hand, the 2D-bed case, displayed a simultaneous sequence of transport events over a wide area, with more evident synchronization of movement over adjacent crests and troughs. Synchronized sediment movements were the main contributors to dunes migrating with a uniform velocity. Collectively, these movements maintain the two-dimensional shapes of dunes. This interpretation is supported by the result of our preliminary experiment in which a similar bedform, dune length/height, and sediment rate were observed four-times in the repeated experiment for the flow condition corresponding to the 2D-bed case. Less reproducibility of bedforms and sediment rates in the preliminary experiment occurred under the 3D-bed case condition and may be due to sporadic sediment transport events occurring on each individual crest observed during the 3D-bed case.

5 Discussion

The recent paper of Muste et al. (2016) introduced a new experimental non-intrusive measurement approach, Acoustic Mapping Velocimetry (AMV), that is based on a combination of acoustic and image based processing protocols. The main idea behind this study was to perform repeated acoustic surveys of a channel bed and to use image velocimetry to detect the movement of clearly recognizable patches on the bed (i.e. bedform migration). The spatial scale for implementation of the AMV is labeled as mesoscale, a scale that is appropriate for the assessment of dune migration. Attempting to resolve finer scale bedforms, such as ripples migrating on dunes, could not be captured with AMV as applied by Muste et al. (2016) due to the lower spatial resolution of the instrumentation used in the experiments. Based on these results, the need for another experimental observation approach that can complement the AMV in fully capturing sediment transport over scales, from individual grains to the larger scale corresponding to bedforms, was realized. The image based methodology presented in this study is a consequence of that realization. The two measurement procedures presented can be combined to provide a better qualitative description for bedform migration from the microscale to the mesoscale.

The technique introduced in this study provides new insights into microscale sediment transport and opens new capabilities for better understanding flow-sediment interactions. For instance, Maddux et al. (2003a) pointed out that the turbulence generated by three-dimensional dunes was weaker as compared to a two-dimensional dune experiment. In our results, sediment transport on two-dimensional dunes displayed more coherent structures (a wider spatial scale and a higher contribution to upper POD modes, as well as a longer wave period for the amplitude coefficients) as compared to results obtained from a three-dimensional dune migration experiment. The difference in the sediment transport pattern may be related and may correspond to the difference in flow turbulence as reported by Maddux et al. (2003a). Based on our knowledge, the capability to capture sediment grain movement over horizontal surfaces covered by sand with an irregular bedform is quite rare. To date, we know of just one study (Naqshband et al., 2017) that has employed a particle-based sediment transport analysis on a rough but almost flat bed.

The goal of this study was to set up a generalized approach and the associated measurement technology for investigating particle transport length, trajectory, and dynamics within a dune length. The results presented in this paper illustrate that the assembled measurement protocols are adequate for quantitatively estimating particle movement across a bedforms' surface, hence linking grain-by-grain displacement to resultant larger scale bedforms that, in turn, affect particle movement over time. The measurement protocol enables verification of the findings related to the translation and deformation of bedforms as determined by McElroy and Mohrig (2009), or the evaluation of dune models that simulate the development and transition of dunes (e.g. Naqshband et al., 2016). While not explored in the current study, the measurement protocol can be extended to more comprehensively analyze particle movement within the uppermost layer of the bedform, uniquely supporting better understanding of the transition between sediment transport modes (i.e. bed-load and suspended load). The reconstruction of sediment movement enabled by the measurement protocol can qualitatively describe resuspension and deposition processes and consequent transport mode changes. If illumination is adequate and if the water is transparent enough to record clear images of the river red, the developed measurement protocol can be applied to on-site measurements in small to medium sized sandy rivers (such as those analyzed in the study of McElroy and Mohrig, 2009). The bedload fluxes were not evaluated in our study here, but could be estimated with the aid of estimating models for the thickness of the bedload transport layer and a bedload concentration.

6 Conclusions

We introduced the innovative combination of an image-based measurement technique using a suite of image processing and post-analysis protocols that provides unique qualitative insights regarding sediment movement within a dune wavelength. Two-dimensional and three-dimensional bedforms were formed in an experimental flume, and sediment particle motion on self-generated bedforms was measured using PIV algorithms, image enhancement, and pre- and post-processing routines. The assembled measurement protocol was enabled to investigate time-averaged patterns and the time-variation of velocity fields for two types of bedforms. The obtained results suggest that concurrent sediment transport over a widespread area occurs on a two-dimensional bedform, whereas sediment transport is sporadic and non-synchronous over adjacent dunes in three-dimensional bedforms. The difference in such spatio-temporal patterns of sediment transport may be a key steering feature for maintaining a uniform dune shape for the two-dimensional bedform case and, at the same time, can account for maintaining the disturbed dune shape for the three-dimensional bedform case.

Our study is exploratory and was aimed at capturing the motion of assemblies for moving particles over dunes rather than quantifying the fluxes of bedload across a flow cross section. Use of this experimental approach allowed us to analyze sediment transport on the basis of the spatially-averaged representative velocity for groups of particles. Experimental limitations (mostly related to the quality of the images) precluded a thorough assessment of associated processes. However, the proposed methodology can be validated using instrumentation with superior fidelity and spatio-temporal resolutions that are readily obtainable (but not available for our study). A potential future direction for advancing the overall protocol is to measure the motion of sediment transport at the level of a particle (rather than for a group of particles) using the Particle Tracking Velocimetry (PTV) approach as employed by, for example, Naqshband et al. (2017) in experiments with quasi flat sediment beds. The experimental approach proof-tested during this study allowed an investigation into the movement of particles over complex bedforms, as independent particles or self-organized in ripples, and related such movement to total bedload flow rates over a variety of bedform geometries.

Acknowledgement

We acknowledge the critical support offered by graduate students H. Xu and H-W. Tsai in conducting laboratory experiments. Valuable practical inputs were received from B. Barquist and J. Niemeyer in assembling various in-house developed components. The first author is grateful to participants at IIHR seminars where he introduced some portions of this study. His effort was partially funded by grants from the Chugoku Civil Engineering Foundation for Mutual Aid, Japan; the Foundation for River and Watershed Environment Management, Japan; and JSPS KAKENHI Grant Numbers JP17K06574 and JP17K06575. Collected and processed laboratory data are available from the corresponding author. The second author acknowledges the support of the ÚNKP-17-4/III, from the New National Excellence Program of the Ministry of Human Capacities, Hungary.

References

Abraham, D., Kuhnle, R. A., & Odgaard, A. J. (2011). Validation of bed-load transport measurements with time-sequenced bathymetric data. *Journal of Hydraulic Engineering, 137*(7), 723–728.

Bennett, S.J. & Best, J.L. (1995) Mean flow and turbulence structure over fixed, two-dimensional dunes: implications for sediment transport and bedform stability, *Sedimentology*, 42, 491–513.

Best, J.L. (2005). The fluid dynamics of river dunes: a review and some future research directions, *Journal of Geophysical Research*, 110, F04S02, DOI 10.1029/2004JF000218.

Cabral, B., & Leedom, L. C. (1993). Imaging vector fields using line integral convolution. In *Proceedings of the 20th annual conference on Computer graphics and interactive techniques,* 263–270, Annual Conference Series.

Cecchetto, M., Tregnaghi, M., Bottacin-Busolin, A., Tait, S., & Marion, A. (2016). Statistical Description on the Role of Turbulence and Grain Interference on Particle Entrainment from Gravel Beds. *Journal of Hydraulic Engineering*, 143(1), 06016021.

Chichibu, K., Watanabe, Y., & Shimizu, Y. (2008). New imaging technique for measuring fluid and solid velocities in sand-laden flows over dunes in an open channel. In Proc. Of 5th IAHR Symposium on River, Coastal and Estuarine Morphodynamics (RCEM 2007), Twente, the Netherlands.

Cizmas, P. G., Palacios, A., O'Brien, T., & Syamlal, M. (2003). Proper-orthogonal decomposition of spatio-temporal patterns in fluidized beds. *Chemical engineering science*, 58(19), 4417–4427.

Constantinescu, G., Balachandran R., Abad, J. & Li, D. (2017). Identification of coherent structures, Section 6.14 in Experimental Hydraulics, Volume I; M. Muste, D.A. Lyn, D.M. Admiraal, R. Ettema, V. Nikora, and M.H. Garcia (Editors); Taylor & Francis, New York, NY.

Detert, M., Weitbrecht, V., & Jirka, G. H. (2010). Laboratory measurements on turbulent pressure fluctuations in and above gravel beds. *Journal of Hydraulic Engineering*, 136(10), 779-789.

Dinehart, R. L. (2002). Bedform movement recorded by sequential single-beam surveys in tidal rivers. *Journal of Hydrology*, *258*(1), 25–39, doi: 10.1016/S0022- 1694(01)00558-3.

Engel, P., & Lau, Y. L. (1981). Bed load discharge coefficient. *Journal of the Hydraulics Division*, *107*(11), 1445-1454.

Feng, L. H., Wang, J. J., & Pan, C. (2011). Proper orthogonal decomposition analysis of vortex dynamics of a circular cylinder under synthetic jet control. *Physics of Fluids*, *23*(1), 014106.

Gunawan, B., Sun, X., Sterling, M., Shiono, K., Tsubaki, R., Rameshwaran, P., Knight, D.K., Chandler, J.H., Tang, X. & Fujita, I. (2012). The application of LS-PIV to a small irregular river for inbank and overbank flows, *Flow Measurement and Instrumentation*, 24, 1-12, doi: 10.1016/j.flowmeasinst.2012.02.001.

Gray, J. R., Laronne, J. B., & Marr, J. D. (2010). *Bedload-surrogate monitoring technologies,* U.S. Geol. Surv. Scientific Investigations Report No. 2010-5091). 37p, US Geological Survey.

Giri, S. & Shimizu, Y. (2006). Numerical computation of sand dune migration with free surface flow, *Water Resources Research*, 42, W10422, doi: 10.1029/2005WR004588.

Heath, R. E., Brown, G. L., Little, C. D., Pratt, T. C., Ratcliff, J. J., Abraham, D. D., Perkey, D., Ganesh, N. B., Martin, K., & May, D. P. (2015). *Old River Control Complex Sedimentation Investigation*, Engineer Research and Development Center/Coastal and Hydraulics Lab. (ERDC/CHL) Technical Report No. TR-15-8).

Hilberg, D., Lazik, W., & Fiedler, H. E. (1994). The application of classical POD and snapshot POD in a turbulent shear layer with periodic structures. *Applied Scientific Research*, 53(3), 283-290.

Kadota, A. & Nezu, I. (1999). Three-dimensional structure of space-time correlation on coherent vortices generated behind dune crest, *Journal of Hydraulic Research*, 37(1), 59–80, doi: 10.1080/00221689909498532.

Kolehmainen, J., Elfvengen. J. & Saarenrinne, P. (2014). Inteference-based overlapping particle tracking velocimetry for fluidized beds, *Experiments in Fluids*, 55, 1825, DOI: 10.1007/s00348-014-1825-2.

Kostaschuk, R. A., Church, M. A., & Luternauer, J. L. (1989). Bedforms, bed material, and bedload transport in a salt-wedge estuary: Fraser River, British Columbia. *Canadian Journal of Earth Sciences*, *26*(7), 1440–1452.

Maddux, T. B., Nelson, J. M., & McLean, S. R. (2003a). Turbulent flow over three-dimensional dunes: 1. Free surface and flow response. *Journal of Geophysical Research: Earth Surface*, 108(F1).

Maddux, T. B., McLean, S. R., & Nelson, J. M. (2003b). Turbulent flow over three-dimensional dunes: 2. Fluid and bed stresses. *Journal of Geophysical Research: Earth Surface*, 108(F1).

McElroy, B., & Mohrig, D. (2009). Nature of deformation of sandy bed forms. *Journal of Geophysical Research: Earth Surface*, *114*(F3), doi: 10.1029/2008JF001220.

Mohrig, D. & Smith J.D. (1996). Predicting the migration rates of subaqueous dunes, *Water Resources Research*, 32(10), 3207–3217 (96WR01129).

Naqshband, S., McElroy, B., & Mahon, R. C. (2017). Validating a universal model of particle transport lengths with laboratory measurements of suspended grain motions. *Water Resources Research*. 53, doi:10.1002/2016WR020024

Naqshband, S., Duin, O., Ribberink, J., & Hulscher, S. (2016). Modeling river dune development and dune transition to upper stage plane bed. *Earth surface processes and landforms*, *41*(3), 323-335, doi: 10.1002/esp.3789.

Nelson, J.M. & Smith, J.D. (1989). Mechanics of flow over ripples and dunes, *Journal of Geophysical Research*, 94, C6, 8146–8162.

Niemann, S. L., J. Fredsøe, and N. G. Jacobsen (2011), Sand dunes in steady flow at low Froude numbers: Dune height evolution and flow resistance, *Journal of Hydraulic Engineering*, 137(1), 5–14, doi:10.1061/(ASCE)HY.1943-7900.0000255.

Palmer J.A, Mejia-Alvarez, R., Best. J.L. & Christensen, K.T. (2012). Particle-image velocimetry measurements of flow over interacting barchans dunes, *Experiments in Fluids*, 52, 809–829, DOI 10.1007/s00348-011-1104-4.

Paarlberg, A.J., Dohmen-Janssen, C.M., Hulscher, S.J.M.H. & Termes, A.P.P. (2006). Modeling river dune evolution using a parameterization of flow separation, *Journal of Geophysical Research*, 114, F01014, doi: 10.1029/2007JF000910.

Simons, D. B., Richardson, E. V., & Nordin, C. F. (1965). *Bedload equation for ripples and dunes*. U.S. Geological Survey Professional Paper 463-H, 1–9.

Sokoray-Varga, B. (2016). Detecting flow events in turbulent flow of vertical-slot fish passes. PhD dissertation. Karlsruhe Institute of Technology. Karlsuhe. Germany.

Tsubaki, R. & Fujita, I. (2005). Stereoscopic measurement of a fluctuating free surface with discontinuities, *Measurement Science and Technology*, 16, 1894-1902.

Tsubaki, R., Nakayama, Y. & Fujita, I. (2008). The design secret of kyokusui-no-en's meandering channel, *Journal of Visualization*, 11(3), 265-272.

Tsubaki, R., Fujita, I. & Tsutsumi, S. (2011). Measurement of the flood discharge of a small-sized river using an existing digital video recording system, *Journal of Hydro-environment Research*, 5(4), 313-321, doi: 10.1016/j.jher.2010.12.004.

Venditti, J. G., Church, M., & Bennett, S. J. (2005). On the transition between 2D and 3D dunes. *Sedimentology*, 52(6), 1343–1359.

Venditti, J. G. (2007). Turbulent flow and drag over fixed two- and three-dimensional dunes. *Journal of Geophysical Research: Earth Surface*, 112(F4).

Wang, H., Gao, Q., Feng, L., Wei, R., & Wang, J. (2015). Proper orthogonal decomposition based outlier correction for PIV data. *Experiments in Fluids*, *56*(2), 43. doi: 10.1007/s00348-015-1894-x.

Westerweel, J., Geelhoed, P. F., & Lindken, R. (2004). Single-pixel resolution ensemble correlation for micro-PIV applications. *Experiments in Fluids*, *37*(3), 375–384.

Yue, W. Lin, C.-L. & Patel, V.C. (2006). Large-eddy simulation of turbulent flow over a fixed two-dimensional dune, *Journal of Hydraulic Engineering*, 132, 643–651.

Zedler, E.A. & Street, R.L. (2001). Large-eddy simulation of sediment transport: currents over ripples, *Journal of Hydraulic Engineering*, 127(6), 444–452.